=========== **NUCLEI** ===========
Theory

Binding Energies of Nuclei and Their Density Distributions in a Nonlocal Extended Thomas−Fermi Approximation

V. Yu. Denisov* and V. A. Nesterov

Institute for Nuclear Research, National Academy of Sciences of Ukraine, pr. Nauki 47, 03680 Kiev, Ukraine

Received April 12, 2000; in final form, May 10, 2001

Abstract—Basic properties of the ground states of spherical nuclei are investigated in a nonlocal extended Thomas−Fermi approximation under the assumption of Skyrme forces. It is shown that, for nuclei occurring near the β-stability line, the binding energies, the root-mean-square radii, and the density distributions found on this basis agree well with experimental data. Binding energies, root-mean-square radii, and density distributions are also calculated for the ground states of nuclei lying far off the β-stability line and for superheavy elements. For the proton, the neutron, and the total particle density, the thickness of the diffuse layer is investigated as a function of the number of neutrons in tin isotopes. © 2002 MAIK "Nauka/Interperiodica".

1. INTRODUCTION

A description of the properties of nuclei in their ground states and low-lying excited states is one of the most important problems in nuclear physics. Over the past decades, theoretical investigations aimed at this have gained a new momentum in connection with the development of phenomenological effective nucleon−nucleon potentials that are expressed in a simple mathematical form [1]. The use of effective Skyrme forces [1] in investigating the properties of nuclear systems facilitates relevant calculations considerably. For the Skyrme forces, a few successful parametrizations were constructed in [2−8], which ensure a description of many nuclear properties to a high precision.

The Hartree−Fock method underlies one of the fundamental approaches to calculating the properties of complex nuclei [2, 3, 5, 6, 8−12]. This quantum-mechanical approach, combined with Skyrme forces, makes it possible to describe well the properties of the ground states of nuclei almost over the entire periodic table of elements [2, 3, 5, 6, 8−10, 12]. Many properties of nuclei were successfully described within Fermi liquid theory [13, 14]. However, an implementation of the Hartree−Fock method and of calculations within Fermi liquid theory in practice involves considerable difficulties. In view of this, use is frequently made of a semiclassical approach that is referred to as the extended Thomas−Fermi approximation [15]. This method is simple, conceptually clear, and rather accurate, which makes it possible

to apply it successfully to describing various physical systems [16]. There is yet another point in favor of using the Thomas−Fermi approximation in calculating basic properties of nuclei: although various modern modifications of the Hartree−Fock approximation are quite fundamental conceptually and elaborate, the most precise description of experimental nuclear masses is provided by simple macroscopic−microscopic approximations [11, 12], which often employ the Thomas−Fermi approximation to calculate the macroscopic part of the binding energy [12].

The extended Thomas−Fermi approximation has been successfully used in atomic and nuclear physics and, since more recent times, in investigations of the properties of metal clusters [17]. Results obtained with the aid of the variational extended Thomas−Fermi approximation for proton-density distributions in nuclei agree well with experimental data, showing slight deviations from them only in the diffuse region [15]. We note that, previously, many properties of nuclei were studied in the local extended Thomas−Fermi approximation [18]; in the nonlocal approximation, this was done by Brack *et al.* [15], whose analysis also involved variations of the parameters in trial functions for nucleon-density distributions.

Under the assumption of Skyrme forces, the nonlocal extended Thomas−Fermi approximation implemented to second-order terms in $\hbar$ [15] is used in the present study to describe the properties of the ground states of medium-mass and heavy spherical nuclei. More specifically, this investigation is performed both for nuclei occurring near the β-stability line and for nuclei lying far off it, as well as for nuclei of superheavy elements. An investigation of nuclei in the

*e-mail: `denisov@kinr.kiev.ua`

vicinity of the presumed stability island around $Z = 114$, $N = 182$ [11, 19] is an especially topical issue, since there have recently appeared reports on the observation of the $Z = 114-116$ and the $Z = 104-112$ nuclei (see [20] and [21], respectively). The equations of the nonlocal extended Thomas–Fermi approximation for the case of Skyrme forces considered in the present study are solved here numerically.

2. EXTENDED THOMAS–FERMI APPROXIMATION

The equations

$$\frac{\delta \mathcal{E}(\rho_n, \rho_p)}{\delta \rho_p} - \lambda_p = 0, \tag{1}$$

$$\frac{\delta \mathcal{E}(\rho_n, \rho_p)}{\delta \rho_n} - \lambda_n = 0 \tag{2}$$

of the extended Thomas–Fermi approximation [15, 16] can be obtained from the variational principle where the total energy of a nucleus is considered as a functional $\mathcal{E}(\rho_n, \rho_p)$ of the neutron density ρ_n and the proton density ρ_p. The possibility of constructing such a functional follows from the Hohenberg–Kohn theorem [22], which is valid for any multicomponent system. The total-energy functional for a nucleus has the form

$$\mathcal{E}(\rho_n, \rho_p) = \int d\mathbf{r}(\tau + \varepsilon_{\text{pot}} + \varepsilon_{\text{Coul}}), \tag{3}$$

where τ, ε_{pot}, and $\varepsilon_{\text{Coul}}$ are the densities of, respectively, the kinetic, the potential, and the Coulomb energy. In Eqs. (1) and (2), λ_n and λ_p are Lagrange multipliers that are chemical potentials for neutrons and protons, respectively, and which are associated with the conservation of the number of neutrons (N) and the number of protons (Z) in a nucleus:

$$\int d\mathbf{r}\rho_{n(p)}(\mathbf{r}) = N(Z). \tag{4}$$

Knowing the expressions for the kinetic, the potential, and the Coulomb energy in (3), one can solve the set of Eqs. (1) and (2) and find the distributions of the neutron and the proton density.

To terms of second order in $\hbar$ [15], the kinetic-energy density is given by

$$\tau = \tau_{\text{TF}} + \tau_2 \tag{5}$$

(the sum of the densities of the kinetic energies of protons and neutrons, $\tau = \tau_p + \tau_n$), where

$$\tau_{\text{TF},n(p)} = k\rho_{n(p)}^{5/3} \tag{6}$$

is the density of the kinetic energy of neutrons (protons) in the Thomas–Fermi approximation ($k =$

$(5/3)(3\pi^2)^{2/3}$) and $\tau_{2n(p)}$ is the second-order gradient correction in $\hbar$ in the nonlocal case [15]. It has the form

$$\tau_{2q} = b_1\frac{(\nabla \rho_q)^2}{\rho_q} + b_2\nabla^2\rho_q + b_3\frac{(\nabla f_q \nabla \rho_q)}{f_q} \tag{7}$$

$$+ b_4\rho_q\frac{\nabla^2 f_q}{f_q} + b_5\rho_q\left(\frac{\nabla f_q}{f_q}\right)^2 + b_6 h_m^2\rho_q\left(\frac{W_q}{f_q}\right)^2,$$

where $q = p$ or n; $b_1 = 1/36$, $b_2 = 1/3$, $b_3 = 1/6$, $b_4 = 1/6$, $b_5 = -1/12$, and $b_6 = 1/2$ are numerical coefficients; and $h_m = \hbar^2/(2m)$. The explicit expressions for the functions f_q and W_q are presented in the Appendix. The last term in Eq. (7) takes into account spin–orbit interaction.

In the case of Skyrme forces, the potential-energy density has the form [1, 2, 10, 15]

$$\varepsilon_{\text{pot}} = \frac{1}{2}t_0\left[\left(1 + \frac{1}{2}x_0\right)\rho^2 - \left(x_0 + \frac{1}{2}\right)\right. \tag{8}$$

$$\times (\rho_n^2 + \rho_p^2)\Big] + \frac{1}{12}t_3\rho^\alpha\left[\left(1 + \frac{1}{2}x_3\right)\rho^2\right.$$

$$- \left(x_3 + \frac{1}{2}\right)(\rho_n^2 + \rho_p^2)\Big] + \frac{1}{4}\left[t_1\left(1 + \frac{1}{2}x_1\right)\right.$$

$$+ t_2\left(1 + \frac{1}{2}x_2\right)\Big]\tau\rho + \frac{1}{4}\left[t_2\left(x_2 + \frac{1}{2}\right)\right.$$

$$- t_1\left(x_1 + \frac{1}{2}\right)\Big](\tau_n\rho_n + \tau_p\rho_p)$$

$$+ \frac{1}{16}\left[3t_1\left(1 + \frac{1}{2}x_1\right) - t_2\left(1 + \frac{1}{2}x_2\right)\right](\nabla\rho)^2$$

$$- \frac{1}{16}\left[3t_1\left(x_1 + \frac{1}{2}\right) + t_2\left(x_2 + \frac{1}{2}\right)\right]$$

$$\times ((\nabla\rho_p)^2 + (\nabla\rho_n)^2)$$

$$+ \frac{1}{2}W_0[\mathbf{J}\nabla\rho + \mathbf{J}_n\nabla\rho_n + \mathbf{J}_p\nabla\rho_p],$$

where t_0, t_1, t_2, t_3, x_0, x_1, x_2, x_3, α, and W_0 are the parameters of the Skyrme potential; $\rho = \rho_n + \rho_p$; $\tau = \tau_n + \tau_p$; $\mathbf{J} = \mathbf{J}_n + \mathbf{J}_p$; and

$$\mathbf{J}_{n(p)} = -\frac{h_m}{f_{n(p)}}\rho_{n(p)}\mathbf{W}_{n(p)}. \tag{9}$$

With allowance for the exchange term, the Coulomb energy density is given by [15, 17]

$$\varepsilon_{\text{Coul}} = \frac{1}{2}e^2\rho_p(\mathbf{r})\int d\mathbf{r}'\frac{\rho_p(\mathbf{r}')}{|\mathbf{r} - \mathbf{r}'|} \tag{10}$$

$$- \frac{3}{4}e^2\left(\frac{3}{\pi}\right)^{1/3}\rho_p^{4/3}(\mathbf{r}).$$

Table 1. Binding energies E, root-mean-square radii $\langle r \rangle$, and chemical potentials λ of β-stable nuclei (experimental values E_{expt} and $\langle r_p \rangle_{\mathrm{expt}}$ were borrowed from [24])

Nucleus	E_{expt}, MeV	E, MeV	$\langle r_p \rangle_{\mathrm{expt}}$, fm	$\langle r_p \rangle$, fm	$\langle r_n \rangle$, fm	λ_n, MeV	λ_p, MeV
[40]Ca	342.1	340.7	3.450	3.186	3.230	-12.12	-10.61
[48]Ca	416.1	418.1	3.451	3.322	3.499	-6.14	-18.86
[58]Ni	506.45	506.1	3.769	3.560	3.617	-11.23	-11.53
[90]Zr	783.9	790.2	4.258	4.069	4.170	-8.62	-14.53
[114]Sn	971.6	982.6	4.602	4.389	4.491	-8.34	-14.41
[140]Ce	1172.7	1182.8	–	4.681	4.817	-6.59	-16.63
[208]Pb	1636.5	1639.8	5.503	5.330	5.486	-5.27	-17.45

Taking into account (3)–(10) and considering the spherically symmetric case, we can recast Eqs. (1) and (2) into the form

$$A_{nn}\nabla^2 \rho_n + A_{np}\nabla^2 \rho_p + B_{nn}(\nabla \rho_n)^2 \quad (11)$$
$$+ B_{np}(\nabla \rho_p)^2 + D_{np}(\nabla \rho_n \nabla \rho_p) + F_n + \lambda_n = 0,$$

$$A_{pp}\nabla^2 \rho_p + A_{pn}\nabla^2 \rho_n + B_{pp}(\nabla \rho_p)^2 \quad (12)$$
$$+ B_{pn}(\nabla \rho_n)^2 + D_{pn}(\nabla \rho_p \nabla \rho_n) + F_p + C + \lambda_p = 0,$$

where A, B, C, D, and F are functions of the variable r. The explicit expressions for them are presented in the Appendix. The coefficient C in Eq. (12) stems from taking into account the Coulomb interaction between intranuclear protons.

The set of Eqs. (11) and (12) is a set of nonlinear integro-differential equations in partial derivatives. In order to solve it in a spherically symmetric case, we make use of the method of successive approximations. The iterative process is continued until the change in the chemical potential upon going over from one iteration to the subsequent one becomes small (specifically, $\delta\lambda_q/\lambda_q \leq 10^{-4}$).

For a zero approximation to the density distribution in the spherically symmetric case, we take the form

$$\rho_q(r) = \rho_{0q}/[1 + \exp((r - R)/a)], \quad (13)$$

where $R = 1.2A^{1/3}$ fm, $a = 0.6$ fm, and ρ_{0q} is the normalization constant determined with the aid of Eq. (4). If we assume that the proton and the neutron density decrease at infinity according to the same law, the large-r asymptotic behavior of the densities is given by

$$\rho_q(r)|_{r\to\infty} = r^{-2} \exp\left(-\sqrt{|\lambda_q|/(h_m b_1)}\,r\right). \quad (14)$$

At the point $r = 0$, the proton and the neutron density must be bounded.

Prior to proceeding to solve the set of Eqs. (11) and (12) numerically, it is convenient to make the change of variables $\rho_q = y_q/r$, which simplifies these equations somewhat. Since ρ_q is bounded at the point $r = 0$, the function $y_q(r)$ satisfies the condition

$$y_q(0) = 0. \quad (15)$$

In order to solve the set of Eqs. (11) and (12) numerically, use was made of the Numerov method in the summed form [23], whereby the computational scheme was stabilized to the maximum possible extent.

3. DISCUSSION OF NUMERICAL RESULTS

We begin the discussion of our numerical results by considering the binding energies of spherical nuclei occurring in the β-stability valley, such as [40]Ca, [48]Ca, [58]Ni, [90]Zr, [114]Sn, [140]Ce, and [208]Pb. In computing the binding energies, we employed the *SIII* [3], *SkM** [5], *T6* [7], *SkP* [6], and *SLy4* [8] parametrizations of the Skyrme forces. Figure 1 shows the relative deviations $(E - E_{\mathrm{expt}})/E_{\mathrm{expt}}$ of the computed binding energies E from their experimental counterparts E_{expt} versus the number of nucleons in the nuclei being considered. The experimental values of the nuclear binding energies were borrowed from [24]. As can be seen from Fig. 1, the calculations with the *SkP* potential reproduce the experimental binding energies most closely. For this reason, the computed binding energies, root-mean-square radii, and chemical potentials are presented in Table 1 only for the *SkP* parametrization.
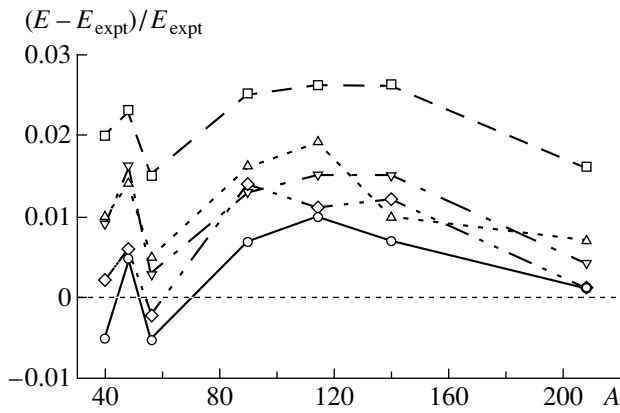
Fig. 1. Relative deviations $(E - E_{\text{expt}})/E_{\text{expt}}$ of the computed nuclear binding energies from their experimental counterparts for the (boxes) *SIII*, (inverted triangles) *SkM**, (triangles) *T6*, (circles) *SkP*, and (diamonds) *SLy4* parametrizations of the Skyrme forces.

It should be noted that, for the majority of the nuclei quoted in Fig. 1, the computed binding energies are slightly in excess of their experimental counterparts. As a rule, the inclusion of shell corrections [11] enhances this effect since, for the majority of the spherical models considered in the present study, the shell correction either increases the binding energy or is close to zero [25]. It follows that, for the majority of the nuclei quoted in Fig. 1, the results that the extended Thomas–Fermi approximation with the *SkP* potential yields for the binding energies with allowance for shell corrections will also be close to the corresponding experimental values.

The values calculated here within the extended version of the Thomas–Fermi approximation for the binding energies and the root-mean-square radii agree well with available experimental data (see Table 1).

The binding energies, root-mean-square radii, and chemical potentials computed here were obtained in the nonlocal approximation. In the local approximation, the coefficients b_2, b_3, and b_4 in Eq. (7) vanish; that is, three gradient terms are discarded, which leads to an additional contribution to the nuclear binding energy. As a result, the nuclear binding energy computed in the nonlocal approximation differs from that which was obtained in the local approximation by a few tenths of a megaelectronvolt in light nuclei and by about 1 MeV in heavy nuclei.

In Fig. 2, the proton densities computed for ^{48}Ca and ^{208}Pb are contrasted against their experimental counterparts. Here and below, the experimental radial distributions of the charge density in nuclei were taken from the analysis of inelastic electron scattering on nuclei as given in [26]. From the results presented in Fig. 2, it follows that the computed proton densities
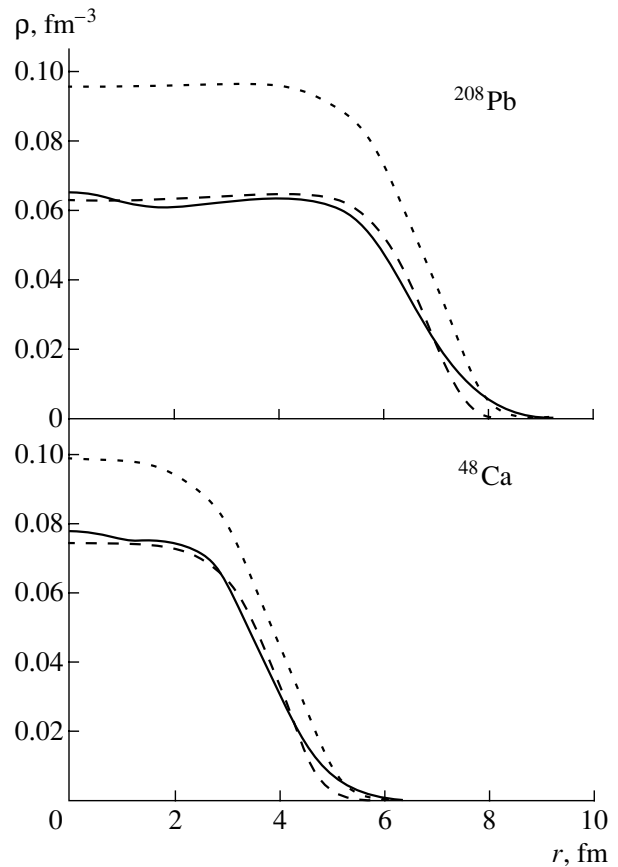

Fig. 2. Radial distributions of (dashed curves) the proton $[\rho_p(r)]$ and (dotted curves) the neutron $[\rho_n(r)]$ density according to the calculations within the extended Thomas–Fermi approximation and (solid curves) experimental proton densities in ^{48}Ca and ^{208}Pb. The experimental charge densities were borrowed from [26].

agree well with the experimental densities in the interior of the nuclei, but that there are slight distinctions in the diffuse region, especially in the region of the distribution tail. These distinctions can be removed by replacing the value of $b_1 = 1/36$ by a greater value— for example, by the quantum-mechanical value of $b_1 = 1/9$ [15]. This replacement improves considerably the density profile, but it reduces significantly the binding energy [15]. The fact that the description of the proton-density profile within the nonlocal extended Thomas–Fermi approximation, which takes into account $\hbar^2$ terms in the kinetic-energy functional, is insufficiently accurate affects the root-mean-square radii as well, which appear to be slightly underestimated (see Table 1).

Having demonstrated that, for spherical nuclei from the region around the β-stability line, the extended Thomas–Fermi approximation provides an accurate description of their gross properties, we now proceed to consider nuclei lying far off the stability
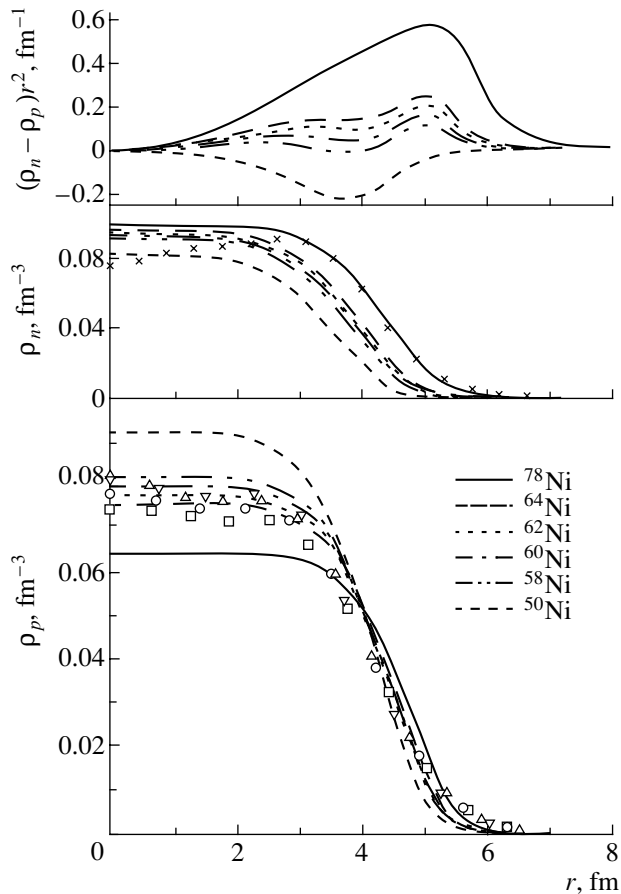
Fig. 3. Radial distributions of the proton $[\rho_p(r)]$ and the neutron $[\rho_n(r)]$ density according to the calculations within the extended Thomas−Fermi approximation, $(\rho_n(r) - \rho_p(r))r^2$, and experimental proton densities for nickel isotopes (data for ^{64}Ni, ^{62}Ni, ^{60}Ni, and ^{58}Ni are represented by boxes, circles, triangles, and inverted triangles, respectively). The experimental charge densities were borrowed from [26]. The radial distribution of neutrons in ^{78}Ni according to the calculations within the relativistic Hartree−Bogolyubov approximation (crosses) was taken from [30].

line, such as ^{32,56}Ca, ^{48,78}Ni, and ^{100,132}Sn. The binding energies, root-mean-square radii, and chemical potentials computed for these nuclei within the extended Thomas−Fermi approximation are quoted in Table 2. The experimental value of the binding energy of the ^{100}Sn isotope was taken from [27]; for the remaining isotopes, the binding energies were borrowed from [24]. We note that the ^{40,48}Ca, ^{48,78}Ni, and ^{100,132}Sn nuclei, for which some features are presented in Tables 1 and 2 and in Figs. 1−4, are doubly magic. The doubly magic nucleus ^{48}Ni was synthesized quite recently [28]. Our computed value of 346.8 MeV for the binding energy of this nucleus agrees well with the result (349.0 MeV) obtained in [29] from a systematics of binding energies.

As can be seen from Table 2, the binding energies calculated within the extended Thomas−Fermi approximation for nuclei lying far off the β-stability line agree well with their experimental counterparts. This indicates that the extended Thomas−Fermi approximation is a highly accurate method for computing the ground-state properties of spherical nuclei.

For the nickel isotopes, the results of the calculations for the density distributions are displayed in Fig. 3, where we can see that, in the interior of the ^{50}Ni and ^{78}Ni nuclei, the proton and neutron densities differ considerably. In the surface layer, there is an excess of proton density (proton skin) in ^{50}Ni; on the contrary, ^{78}Ni has a neutron skin. We note that the proton and the neutron density in the interior of nuclei change considerably upon going over from neutron-deficient to neutron-rich isotopes, the total particle density at the center of a nucleus remaining virtually unchanged. The results that we obtained for the proton-density distributions agree well with experimental data from [26], while our result for the neutron-density distribution in the ^{78}Ni nucleus comply with the results of microscopic calculations performed within the relativistic Hartree−Bogolyubov approximation [30].

For tin isotopes, the radial dependences of the proton and neutron densities are displayed in Fig. 4. The shapes of the densities for neutron-deficient and neutron-rich tin isotopes are identical to those for nickel isotopes.

From Figs. 3 and 4, it can be seen that the radial proton-density distributions computed in the extended Thomas−Fermi approximation comply well with experimental data (for the Ni and Sn isotopes presented in these figures) in the interior of the nuclei and slightly differ from them in their surface regions.

Within the extended Thomas−Fermi approximation, it is possible to assess the position of the line of neutron stability of the elements. As can be seen from Fig. 5, the chemical potentials computed within the extended Thomas−Fermi approximation for Ni and Sn isotopes change smoothly in response to variations in the number of neutrons. The neutron number at which the chemical potential changes sign from a negative to a positive one corresponds to the boundary of neutron stability of an element. The extended Thomas−Fermi approximation is a macroscopic approach taking no account of either the shell structure of the nucleus or pairing effects; therefore, it can yield only an approximate position for the boundary of neutron stability of the elements. Nonetheless, the value computed here on this basis for tin isotopes ($A = 162$) is in satisfactory agreement with the value found within the model proposed in [25] ($A = 157$). Moreover, our curves comply well with the results of calculations within the relativistic Hartree−Bogolyubov

Table 2. Binding energies E, root-mean-square radii $\langle r \rangle$, and chemical potentials λ of neutron-rich and neutron-deficient nuclei (the experimental values E_{expt} were taken from [27] for ^{100}Sn and from [24] for the remaining isotopes)

Nucleus	E_{expt}, MeV	E, MeV	$\langle r_p \rangle$, fm	$\langle r_n \rangle$, fm	λ_n, MeV	λ_p, MeV
^{32}Ca	−	201.5	3.100	2.922	−22.470	−0.590
^{56}Ca	449.6	456.0	3.447	3.754	−2.440	−25.248
^{48}Ni	−	346.8	3.433	3.328	−19.707	−2.521
^{50}Ni	385.5	385.7	4.453	4.389	−17.643	−4.431
^{60}Ni	526.9	528.9	3.589	3.670	−9.991	−13.153
^{62}Ni	545.3	549.4	3.618	3.723	−8.854	−14.694
^{64}Ni	561.8	567.6	3.646	3.774	−7.825	−16.184
^{78}Ni	641.4	646.8	3.833	4.124	−2.572	−24.853
^{100}Sn	825.8	819.7	4.243	4.247	−13.37	−7.84
^{124}Sn	1049.4	1060.0	4.491	4.655	−5.702	−18.480
^{132}Sn	1102.7	1104.0	4.568	4.783	−3.981	−21.352

Table 3. Binding energies E, root-mean-square radii $\langle r \rangle$, and chemical potentials λ computed for superheavy nuclei within the extended Thomas−Fermi approximation and binding energies E_{TF} obtained in the Thomas−Fermi approximation [32]

Z	N	E, MeV	E_{TF}, MeV	$\langle r_p \rangle$, fm	$\langle r_n \rangle$, fm	λ_n, MeV	λ_p, MeV
114	182	2121.6	2099.8	6.006	6.536	−4.777	−16.640
118	182	2132.1	2109.9	6.040	6.176	−5.418	−15.347
120	182	2134.9	2112.7	6.061	6.210	−6.064	−13.711
126	182	2134.2	2112.32	6.107	6.209	−6.692	−11.855
126	184	2149.4	2127.50	6.119	6.225	−6.482	−13.190
164	272	2667.9	−	6.686	7.012	−4.303	−15.003
164	318	2847.6	−	7.080	7.315	−1.716	−19.907

approximation [30] (see Fig. 5). For Ni isotopes, the computed value of $A = 90$ agrees well with the value obtained within the relativistic Hartree−Bogolyubov approximation ($A = 94$) [30] and with the value found in the three-dimensional Hartree−Fock−Bogolyubov approximation [31].

Let us now proceed to investigate the ground-state properties of superheavy elements in the region of the possible stability island around $Z = 114$, $N = 184$. We will also consider the $Z = 164$, $N = 272$, 318 nuclei. It should be noted that the magic number of $Z = 114$ was obtained within various models [11, 19]. The $Z \approx 114$ and $N \approx 182$ nuclei have a spherical shape or a shape close to it [19].

The stability of superheavy nuclei is associated with the shell correction, owing to which there is a fission barrier in these nuclei [11, 19, 21]. However, the effect of the shell correction on the density distributions in nuclei occurring close to the β-stability line is insignificant. Moreover, it is necessary to know the macroscopic binding energy in order to calculate the total binding energy of nuclei by the shell-correction method. Therefore, it is of great interest to investigate, within the extended Thomas−Fermi approximation, the density distributions in superheavy nuclei and their macroscopic binding energies.

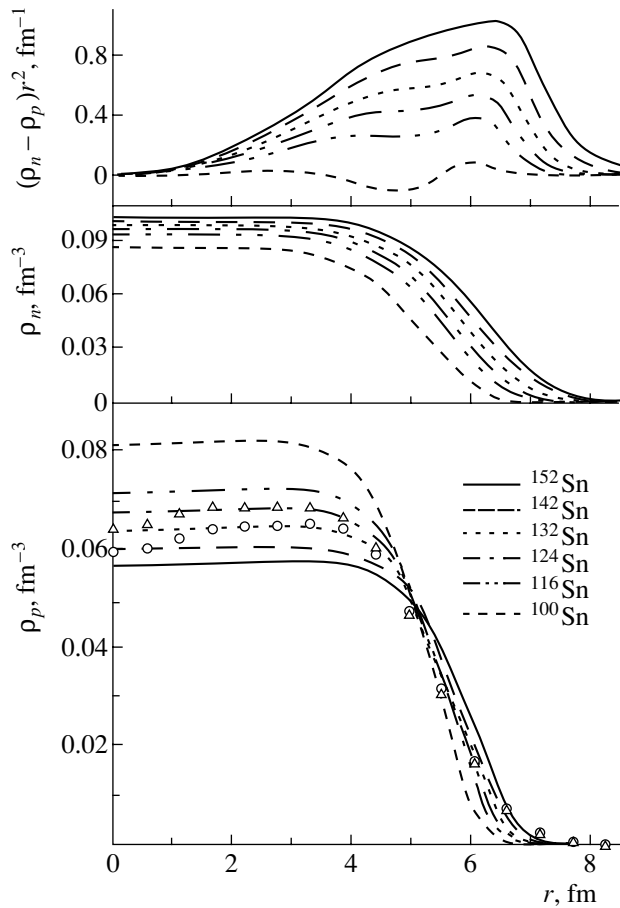For the ground-state properties of the nuclei of superheavy elements, the results of the calculations

Fig. 4. Radial distributions of the proton $[\rho_p(r)]$ and the neutron $[\rho_n(r)]$ density according to the calculation within the extended Thomas–Fermi approximation, $(\rho_n(r) - \rho_p(r))r^2$, and experimental proton densities for tin isotopes (data for ^{124}Sn and ^{116}Sn are represented by circles and triangles, respectively). The experimental charge densities were borrowed from [26].

Fig. 5. Proton and neutron chemical potentials versus the number of neutrons for nickel and tin isotopes. The results of the calculations within the relativistic Hartree–Bogolyubov approximation [30] (circles) and the experimental values of the neutron-separation energies [24] (crosses) are also presented here for the sake of comparison.

with the *SkP* potential are presented in Table 3. The results of the calculations with the *SkM** and *SLy4* potentials agree within 1% with the results quoted in this table. In the region of the nuclei being considered, the Coulomb repulsion is so strong that the binding energy of the nuclei changes only slightly in response to an increase in the number of protons at a fixed number of neutrons ($N = 182$). From the values of λ_n quoted in Table 3, it can be seen that the superheavy nuclei must be stable with respect to neutron emission. For superheavy nuclei, Table 3 also gives the binding energies that were obtained in the Thomas–Fermi approximation for the case of finite-range forces [32]. The parameters of these forces were chosen in [32] in such a way as to reproduce the experimental nuclear masses. From Table 3, it can be seen that the binding energies computed for super-heavy nuclei in the extended Thomas–Fermi approx-
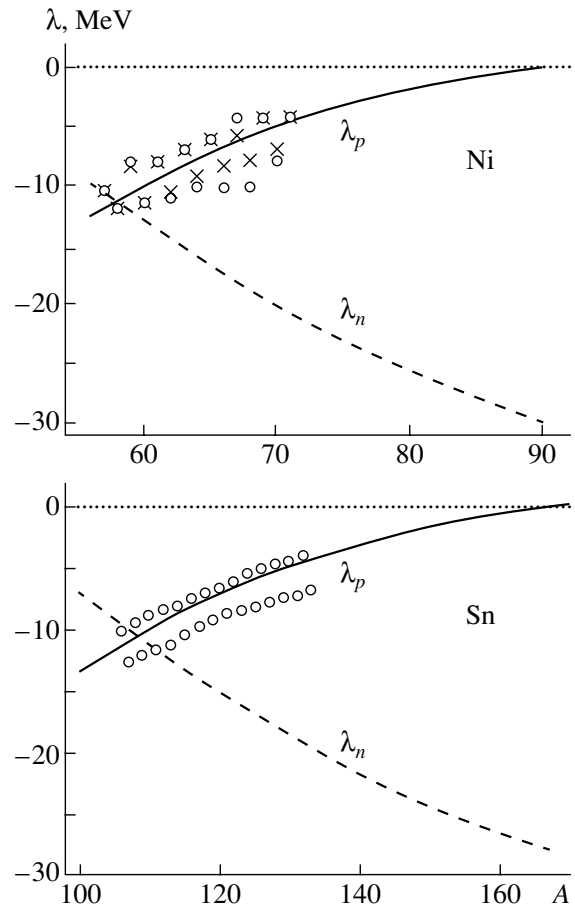
imation with the *SkP* forces are greater than those found in [32], this difference significantly exceeding the typical value of the shell correction for these nuclei [19, 21, 25, 32].

Figure 6 displays the distributions of the proton and the neutron density for the $^{292,300}_{120}$X and $^{482}_{168}$X nuclei. As can be seen from Fig. 6, the Coulomb repulsion leads to a significant displacement of the intranuclear protons to the periphery of the nuclei. The proton density in the interior of the nuclei is lower than at their surfaces and in the intermediate region between the periphery and the interior.

We define the thickness of the diffuse layer, t, for a density distribution as the distance over which the density changes from 90 to 10% of its maximum value. Figure 7 displays the thicknesses of the diffuse layer for the proton (t_p), the neutron (t_n), and the total particle (t_{tot}) density versus the number of neutrons
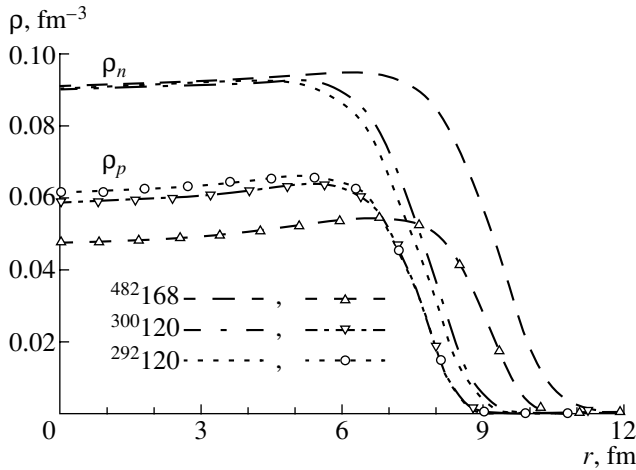
ρ, fm^{-3}

Fig. 6. Radial distributions of the proton and the neutron density in the nuclei of superheavy elements according to the calculations within the extended Thomas−Fermi approximation.
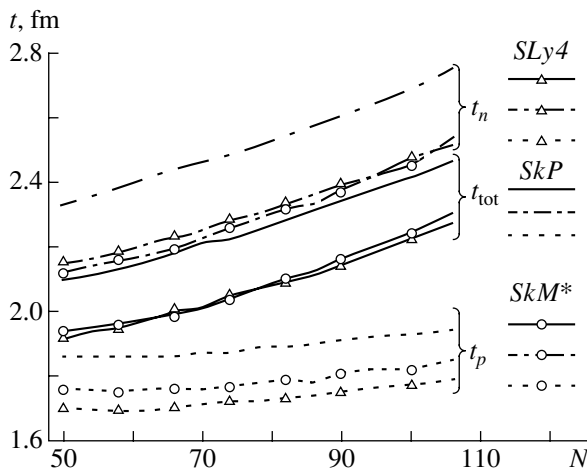

Fig. 7. Thicknesses of the diffuse layer for the proton (t_p), the neutron (t_n), and the total particle (t_{tot}) density in tin isotopes versus the number of neutrons (N) according to the calculations with the *SLy4*, the *SkP*, and the *SkM** parametrization.

in tin isotopes. The thicknesses of the diffuse layer that are presented in Fig. 7 were computed within the extended Thomas−Fermi approximation by using the *SLy4*, *SkP*, and *SkM** parametrizations of the Skyrme forces. From Fig. 7, it can be seen that the thickness of the diffuse layer increases with increasing number of neutrons. A similar type of behavior of the diffuse layer in these nuclei was also found within microscopic calculations [33]. At the same time, the quantity t_p remains virtually unchanged, the growth of t_{tot} with increasing number of neutrons being due to the growth of t_n. This behavior of the neutron

density in various tin isotopes is expected to manifest itself in nuclear reactions that are sensitive to the distribution of neutrons.

4. CONCLUSION

It has been shown that the nonlocal extended Thomas−Fermi approximation implemented for the case of Skyrme forces appears to be a simple, fairly accurate, and efficient means for studying the ground-state properties of medium-mass and heavy nuclei, both those occurring near the β-stability line and those lying far off it. The calculated binding energies of stable and unstable nuclei closely reproduce experimental data. A good description of the root-mean-square charge radii has also been obtained. The results of the calculations within the extended Thomas−Fermi approximation for the radial distributions of the proton densities agree well with the experimental distributions in the interior of nuclei and slightly deviate from them in the diffuse region. The ground states of superheavy nuclei have been considered. It has been found that, in the $Z \approx 114-120$ superheavy nuclei, there is a modest decrease in the density at the center of a nucleus. The thicknesses of the diffuse layer for the total particle density and for the neutron density have been shown to increase with increasing number of neutrons in nuclei.

ACKNOWLEDGEMENTS

APPENDIX

The functions $f_{p(n)}$ and $\mathbf{W}_{n(p)}$ introduced in (7) are given by

$$f_{n(p)} = 1 + h_m[(\gamma + \beta)\rho_{n(p)} + \gamma\rho_{p(n)}],$$

$$f'_{np(pn)} = h_m\gamma, \quad f'_{nn(pp)} = h_m(\gamma + \beta),$$

$$\mathbf{W}_{n(p)} = \frac{W_0}{2}[2\nabla\rho_{n(p)} + \nabla\rho_{p(n)}],$$

where

$$\gamma = \frac{1}{4}\left[t_1\left(1 + \frac{1}{2}x_1\right) + t_2\left(1 + \frac{1}{2}x_2\right)\right],$$

$$\beta = \frac{1}{4}\left[t_2\left(x_2 + \frac{1}{2}\right) - t_1\left(x_1 + \frac{1}{2}\right)\right].$$

The coefficients in Eqs. (11) and (12) can be represented as

$$A_{pp} = \frac{2}{h_m}\left(f'_{pp}(b_2 - b_3 + b_4) - b_1\frac{f_p}{\rho_p} - C_{pp}\frac{\rho_p}{f_p}\right)$$

$$-\bar{C}_{np}\frac{\rho_n}{f_n}\bigg) + 2h_m a_9^2\left(4\frac{\rho_p}{f_p} + \frac{\rho_n}{f_n}\right) - 2(a_7 + a_8),$$

$$A_{pn} = \frac{2}{h_m}\left(f'_{pn}(b_2 - b_3 + b_4) - C_{pn}\left(\frac{\rho_p}{f_p} + \frac{\rho_n}{f_n}\right)\right)$$

$$-2a_7 + 4h_m a_9^2\left(\frac{\rho_p}{f_p} + \frac{\rho_n}{f_n}\right),$$

$$B_{pp} = \frac{1}{h_m}\left(b_1\frac{f_p}{\rho_p^2}F_{pp} - C_{pp}\frac{F_{pp}}{f_p} + \bar{C}_{np}f'_{np}\frac{\rho_n}{f_n^2}\right)$$

$$+ h_m a_9^2\left(4\frac{F_{pp}}{f_p} - f'_{np}\frac{\rho_n}{f_n^2}\right),$$

$$B_{pn} = \frac{1}{h_m}\left(\bar{C}_{pn}\frac{F_{pp}}{f_p} + b_1\frac{f'_{np}}{\rho_n} - C_{nn}\frac{f'_{np}}{f_n^2}\rho_n\right.$$

$$\left.+ 2C_{pn}f'_{pn}\frac{\rho_p}{f_p^2} - 2C_{pn}\frac{F_{nn}}{f_n}\right)$$

$$+ h_m a_9^2\left(-\frac{F_{pp}}{f_p} + 4\frac{F_{nn}}{f_n} - 4f'_{pn}\frac{\rho_p}{f_p^2} + 4f'_{np}\frac{\rho_n}{f_n^2}\right),$$

$$D_{pn} = \frac{2}{h_m}\left(-f'_{pn}\frac{b_1}{\rho_p} + C_{pp}f'_{pn}\frac{\rho_p}{f_p^2} - \bar{C}_{np}\frac{F_{nn}}{f_n}\right)$$

$$+ 2h_m a_9^2\left(\frac{F_{nn}}{f_n} - 4f'_{pn}\frac{\rho_p}{f_p^2}\right),$$

$$F_p = \frac{k}{h_m}\left(f'_{pp}\rho_p^{5/3} + \frac{5}{3}f_p\rho_p^{2/3} + f'_{np}\rho_n^{5/3}\right)$$

$$+ 2a_1(\rho_n + \rho_p) + 2a_2\rho_p + (\alpha + 2)a_3(\rho_n + \rho_p)^{\alpha+1}$$

$$+ \alpha a_4(\rho_n + \rho_p)^{\alpha-1}(\rho_n^2 + \rho_p^2) + 2a_4\rho_p(\rho_n + \rho_p)^\alpha,$$

$$C = 2\pi e^2\left(\frac{1}{r}\int_0^r r'^2\rho_p(r')dr' + \int_r^\infty r'\rho_p(r')dr'\right)$$

$$- e^2\left(\frac{3\rho_p(r)}{\pi}\right)^{1/3},$$

where we have introduced the following notation:

$$F_{nn(pp)} = 1 - \rho_{n(p)}f'_{nn(pp)}/f_{n(p)},$$

$$C_{nn(pp)} = b_5 f'^2_{nn(pp)} + 4b_6 h_m^2 a_9^2,$$

$$C_{np(pn)} = b_5 f'_{nn(pp)}f'_{np(pn)} + 2b_6 h_m^2 a_9^2,$$

$$\bar{C}_{np(pn)} = b_5 f'^2_{np(pn)} + b_6 h_m^2 a_9^2,$$

$$C_{nn} = C_{pp}, \quad C_{np} = C_{pn}, \quad \bar{C}_{np} = \bar{C}_{pn},$$

$$a_1 = 0.5t_0(1 + 0.5x_0), \quad a_2 = -0.5t_0(x_0 + 0.5),$$

$$a_3 = t_3(1 + 0.5x_3)/12, \quad a_4 = -t_3(x_3 + 0.5)/12,$$

$$a_7 = (3t_1(1 + 0.5x_1) - t_2(1 + 0.5x_2))/16,$$

$$a_8 = -(3t_1(0.5 + x_1) + t_2(0.5 + x_2))/16,$$

$$a_9 = 0.5W_0.$$

The corresponding coefficients for Eq. (12) are obtained upon the interchange of n and p.

REFERENCES

1. T. H. R. Skyrme, Nucl. Phys. **9**, 635 (1959).
2. D. Vatherin and D. Brink, Phys. Rev. C **5**, 626 (1972).
3. M. Beiner, H. Flocard, N. V. Giai, and P. Quentin, Nucl. Phys. A **238**, 29 (1975).
4. Nguyen Van Giai and N. Sagawa, Nucl. Phys. A **371**, 1 (1981).
5. J. Bartel, P. Quentin, M. Brack, *et al.*, Nucl. Phys. A **386**, 79 (1982).
6. J. Dobaczewski, H. Flocard, and J. Treiner, Nucl. Phys. A **422**, 103 (1984).
7. F. Tondeur, M. Brack, M. Farine, and J. M. Pearson, Nucl. Phys. A **420**, 297 (1984).
8. E. Chabanat, PhD Thesis (Lyon, 1995); E. Chabanat, P. Bonche, P. Haensel, *et al.*, Nucl. Phys. A **635**, 231 (1998).
9. B. I. Barts, Yu. L. Bolotin, E. V. Inopin, and V. Yu. Gonchar, *Hartree-Fock Method in Nuclear Theory* (Naukova Dumka, Kiev, 1982).
10. P.-G. Reinhard, D. J. Dean, W. Nazarewicz, *et al.*, Phys. Rev. C **60**, 014316 (1999).
11. V. M. Strutinsky, Nucl. Phys. A **95**, 420 (1967); **122**, 1 (1968).
12. Z. Patyk, A. Baran, J. F. Berger, *et al.*, Phys. Rev. C **59**, 704 (1999).
13. A. B. Migdal, *Theory of Finite Fermi Systems and Applications to Atomic Nuclei* (Nauka, Moscow, 1983, 2nd ed.; Interscience, New York, 1967).
14. É. E. Sapershteĭn and V. A. Khodel', Izv. Akad. Nauk SSSR, Ser. Fiz. **47**, 907 (1983).
15. M. Brack, C. Guet, and H.-B. Hakanson, Phys. Rep. **123**, 275 (1985).
16. M. Brack and R. K. Bhaduri, *Semiclassical Physics* (Addison-Wesley, Reading, 1997).
17. M. Brack, Rev. Mod. Phys. **65**, 677 (1993).
18. V. M. Kolomiets, *Local-Density Approximation in Atomic and Nuclear Physics* (Naukova Dumka, Kiev, 1990).
19. R. Smolanczuk, J. Skalski, and A. Sobiczewski, Phys. Rev. C **52**, 1871 (1995); R. Smolanczuk, Phys. Rev. C **56**, 812 (1997).
20. Yu. Ts. Oganessian *et al.*, Phys. Rev. Lett. **83**, 3154 (1999); Yad. Fiz. **63**, 1769 (2000) [Phys. At. Nucl. **63**, 1679 (2000)]; Yad. Fiz. **64**, 1427 (2001) [Phys. At. Nucl. **64**, 1349 (2001)].
21. G. Münzenberg, Rep. Prog. Phys. **51**, 57 (1988); S. Hofmann, Rep. Prog. Phys. **61**, 373 (1998); G. N. Flerov, I. Zvara, G. M. Ter-Akopyan, *et al.*, Fiz. Élem. Chastits At. Yadra **22**, 931 (1991) [Sov. J. Part. Nucl. **22**, 453 (1991)].
22. P. Hohenberg and W. Kohn, Phys. Rev. **136**, B864 (1964).
23. Liviu Gr. Iharu, *Numerical Methods for Differential Equations and Applications* (Editura Academiei, Bucharest, 1984).

24. G. Audi, O. Bersillon, J. Blachot, and A. H. Wapstra, Nucl. Phys. A **624**, 1 (1997); G. Audi and A. H. Wapstra, Nucl. Phys. A **595**, 409 (1995).
25. P. Moller, J. R. Nix, and K.-L. Kratz, At. Data Nucl. Data Tables **66**, 131 (1997); P. Möller, J. R. Nix, W. D. Myers, and W. J. Swiatecki, At. Data Nucl. Data Tables **59**, 185 (1995).
26. H. De Vries, C.W. De Jager, and C. De Vries, At. Data Nucl. Data Tables **36**, 495 (1987).
27. M. Chartier *et al.*, Phys. Rev. Lett. **77**, 2400 (1996).
28. B. Blank *et al.*, Phys. Rev. Lett. **84**, 1116 (2000).
29. B. A. Brown, Phys. Rev. C **58**, 220 (1998).
30. G. A. Lalazissis, D. Vretenar, and P. Ring, Phys. Rev. C **57**, 2294 (1998).
31. J. Terasaki, P.-H. Heenen, H. Flocard, and P. Bonche, Nucl. Phys. A **600**, 371 (1996).
32. W. D. Myers and W. J. Swiatecki, Nucl. Phys. A **601**, 141 (1996).
33. J. Dobaczewski *et al.*, Phys. Rev. C **53**, 2809 (1996).

Translated by A. Isaakyan